OPEN ACCESS Freely available online

PLoS PATHOGENS

Melanoma Differentiation-Associated Gene 5 (MDA5) Is Involved in the Innate Immune Response to *Paramyxoviridae* Infection In Vivo

Leonid Gitlin[1☯], Loralyn Benoit[2☯], Christina Song[1], Marina Cella[1], Susan Gilfillan[1], Michael J. Holtzman[2,3], Marco Colonna[3]*

1 Department of Pathology and Immunology, Washington University School of Medicine, St. Louis, Missouri, United States of America, **2** Pulmonary and Critical Care Medicine, Department of Internal Medicine, Washington University School of Medicine, St. Louis, Missouri, United States of America, **3** Department of Cell Biology and Physiology, Washington University School of Medicine, St. Louis, Missouri, United States of America

Abstract

The early host response to pathogens is mediated by several distinct pattern recognition receptors. Cytoplasmic RNA helicases including RIG-I and MDA5 have been shown to respond to viral RNA by inducing interferon (IFN) production. Previous in vitro studies have demonstrated a direct role for MDA5 in the response to members of the *Picornaviridae*, *Flaviviridae* and *Caliciviridae* virus families ((+) ssRNA viruses) but not to *Paramyxoviridae* or *Orthomyxoviridae* ((−) ssRNA viruses). Contrary to these findings, we now show that MDA5 responds critically to infections caused by *Paramyxoviridae* in vivo. Using an established model of natural Sendai virus (SeV) infection, we demonstrate that MDA5$^{-/-}$ mice exhibit increased morbidity and mortality as well as severe histopathological changes in the lower airways in response to SeV. Moreover, analysis of viral propagation in the lungs of MDA5$^{-/-}$ mice reveals enhanced replication and a distinct distribution involving the interstitium. Though the levels of antiviral cytokines were comparable early during SeV infection, type I, II, and III IFN mRNA expression profiles were significantly decreased in MDA5$^{-/-}$ mice by day 5 post infection. Taken together, these findings indicate that MDA5 is indispensable for sustained expression of IFN in response to paramyxovirus infection and provide the first evidence of MDA5-dependent containment of in vivo infections caused by (−) sense RNA viruses.

Citation: Gitlin L, Benoit L, Song C, Cella M, Gilfillan S, et al. (2010) Melanoma Differentiation-Associated Gene 5 (MDA5) Is Involved in the Innate Immune Response to *Paramyxoviridae* Infection In Vivo. PLoS Pathog 6(1): e1000734. doi:10.1371/journal.ppat.1000734

Editor: Ralph S. Baric, University of North Carolina, United States of America

Received June 17, 2009; **Accepted** December 21, 2009; **Published** January 22, 2010

Funding: This work was supported by grants from the National Institutes of Health (National Heart, Lung, and Blood Institute and National Institute of Allergy and Infectious Diseases), the Martin Schaeffer Fund, and the Alan A. and Edith L. Wolff Charitable Trust to MJH and JDRF #24-2007-420 to MC. LG is supported by the Cancer Research Institute. LB is supported by NIH/NHLBI training grant T32 HL007317. The funders had no role in study design, data collection and analysis, decision to publish, or preparation of the manuscript.

Competing Interests: The authors have declared that no competing interests exist.

* E-mail: mcolonna@wustl.edu

☯ These authors contributed equally to this work.

Introduction

Innate pathogen sensors detect viral products and respond by initiating a signaling cascade that leads to rapid anti-viral response involving secretion of type I IFNs (i.e. IFN-α and IFN-β) and inflammatory cytokines (i.e. IL-6 and TNF-α) [1]. In particular, type I IFNs restrict infection by inhibiting viral replication within cells and by stimulating the innate and adaptive immune responses. Once induced, secreted IFN-α and IFN-β bind to the IFNα receptor on the cell surface in an autocrine or paracrine manner. Activation of this receptor initiates the JAK/STAT signal transduction pathways [2,3] and the expression of IFN-inducible genes [4]. These gene products increase the cellular resistance to viral infection and sensitize virally-infected cells to apoptosis [5]. In addition, type I IFNs directly activate DC and NK cells, and promote effector functions of T and B cells, thus providing a link between the innate response to infection and the adaptive immune response [6,7].

Several viral sensors have been identified that belong to the Toll-like receptor (TLR) and RIG-I like receptor (RLR) families [8]. TLRs are expressed on the cell surface and/or in endosomal compartments [9]. TLR3 recognizes double stranded RNA (dsRNA), a molecular pattern associated with replication of single stranded RNA (ssRNA) viruses as well as the genomic RNA of dsRNA viruses [10]. TLR7 and TLR8 recognize ssRNA [9,11,12], whereas TLR9 recognizes unmethylated CpG-containing DNA [13]. RLRs are cytoplasmic proteins that recognize viral nucleic acids that have gained access to the cytosol [14–19]. The RLR family consists of three known members: retinoic acid-inducible gene I (RIG-I), melanoma differentiation-associated gene 5 (MDA5), and LGP2. RIG-I and MDA5 both contain a DExD/H box helicase domain that binds dsRNA, a C-terminal domain and two N-terminal caspase recruitment domains (CARDs) that are involved in signaling [8,17,20,21]. LGP2 contains a helicase domain but lacks the CARDs, and its precise contribution to antiviral signaling remains ambiguous [17,22].

Though RIG-I and MDA5 share common downstream signaling via activation of IPS-1 (also called MAVS, VISA or Cardif) and IRF3 [23–26], these helicases exhibit distinct substrate specificity. In this regard, RIG-I has been shown to preferentially

Author Summary

The innate immune system possesses an array of sensory molecules which are purposed in detecting viral nucleic acids. Our understanding of how these molecular sensors detect viral nucleic acids continues to evolve. Herein, we demonstrate that MDA5, a member of the RIG-I-like receptor family, is involved in the detection of paramyxovirus infection in vivo. Specifically, MDA5 appears to trigger antiviral cytokines that inhibit paramyxovirus replication. In this regard, mice that are deficient in MDA5 are unable to express sustained levels of these cytokines and thus succumb to extensive viral propagation and disease. Our findings are largely discordant from previous in vitro studies using cultured cells, where it has been shown that RIG-I and not MDA5 is involved in the innate response to negative sense RNA viruses. Thus, our data provides strong evidence of MDA5-based detection of negative sense RNA viruses, and furthermore underscore the importance of organism-based analysis of the innate system.

recognize ssRNA that is phosphorylated at the 5′ end [27,28] and dsRNA molecules which are relatively short [29–31]. In contrast, MDA5 recognizes long dsRNAs but does not discern 5′ phosphorylation[30,32,33]. This distinct ligand preference has been shown to confer specific recognition of individual viruses: RIG-I has been shown to detect Influenza A and B viruses, paramyxovirus, vesicular stomatitis virus (all (−) ssRNA virues) and some Flaviviruses ((+) ssRNA viruses including Japanese encephalitis virus, Hepatitis C virus and West Nile virus)[16,33,34]. In comparison, MDA5 has been shown to selectively detect (+) ssRNA viruses including picornaviruses (encephalomyocarditis virus, Mengo virus and Theilers virus) [32,33], *Caliciviridae* (murine norovirus-1) [35], and *Flaviviridae* (West Nile Virus and Dengue Virus) [34,36]. Accordingly, it is believed that the presence of different classes of sensors may reflect the need for multiple mechanisms to effectively control the wide variety of viral pathogens.

Paramyxoviruses are (−) ssRNA viruses that are responsible for a number of human diseases including those caused by measles, mumps, parainfluenza virus and respiratory syncytial virus (RSV). Importantly, infections caused by paramyxoviruses are the most frequent cause of serious respiratory illness in childhood and are associated with an increased risk of asthma [37,38]. Sendai virus (SeV) is a murine parainfluenza virus which causes an acute respiratory disease in mice that resembles severe paramyxoviral bronchiolitis found in humans following RSV infection [39]. To date, RIG-I is the only dsRNA sensor that has been implicated in the veritable detection of paramyxoviruses [33,40]. The importance of RIG-I in the containment of SeV infection is underscored by capacity of SeV C proteins to directly antagonize RIG-I signaling [41] in addition to their ability to inhibit IFN signal transduction [42,43]. However, paramyxovirus-encoded V proteins are known to directly interfere with MDA5 function by blocking binding of dsRNA [14,44], thus implicating MDA5 in the containment of paramyxovirus infection as well. In addition, SeV defective interfering (DI) particles have been shown to engage MDA5 in vitro [45], though the in vivo relevancy of this detection mode is unknown. Thus, to determine whether MDA5 functions during natural infection with paramyxovirus in vivo, we assessed mice deficient in MDA5 ($MDA5^{-/-}$ mice) following respiratory tract infection with SeV.

Results

Infection with SeV causes increased morbidity and mortality in $MDA5^{-/-}$ mice

In order to assess an in vivo role for MDA5 in containment of paramyxovirus infection, we infected $MDA5^{-/-}$ mice with Sendai virus (SeV). Mice on a C57BL/6 (B6) background were selected for these experiments as the 129 strain is lethally susceptible to SeV at extremely low inocula [46], thus prohibiting assessment of loss of MDA5 function on this background. A dose of 200,000 pfu was administered to mice by intranasal delivery, an infection method that typically results in acute, non-lethal bronchiolitis in B6 mice. As a gross determinant of virus-induced morbidity, % body weight for infected WT and $MDA5^{-/-}$ mice was monitored for 2 weeks post infection (PI). Though essentially identical % weight loss values were observed up until day 8 PI; onwards, weight loss in $MDA5^{-/-}$ mice was significantly more severe ($p<0.05$) (Figure 1A). Correspondingly, histological analysis of lung sections obtained from day 12 PI $MDA5^{-/-}$ mice revealed consolidation of the lung parenchyma as well as notable PAS-positive airway cells, an indication of mucus hyper-secretion (Figure 1B). Severe histopathology was not observed in the lung sections obtained from control mice at this time point. In addition, we compared survival following increasing inocula of SeV (Figure 1C). Though $MDA5^{-/-}$ mice were not susceptible to the 200K pfu SeV dose, $MDA5^{-/-}$ mice fully succumbed to 400K and 600K pfu SeV, between 9–14 days PI. In contrast, control mice were fully resistant to the 400K pfu dose, though 40% mortality was observed for controls infected with the 600K dose. Thus $MDA5^{-/-}$ mice exhibit enhanced morbidity and susceptibility to SeV infection relative to control mice.

To more fully assess SeV susceptibility, we extended our analysis of the histological changes seen in the lungs of SeV-infected $MDA5^{-/-}$ mice. H&E stained sections obtained from day 2 PI (not shown) and day 5 PI (Figure 2A) lungs demonstrated similar patterns of bronchiolitis, though peribronchiolar lymphoid cuffing that formed in the lungs of control mice appeared moderately thicker and more densely populated than those of $MDA5^{-/-}$ mice (Figure 2A). FACS analysis of lung-derived leukocytes at d2, d5, and d8 PI revealed no significant differences in lymphoid and myeloid subpopulations (neutrophils, cDC, macrophage and alveolar macrophage; data not shown). Significantly, at d5 and d8 PI, FACS analysis revealed equal relative numbers of lymphoid subpopulations ($CD3^+$, $CD19^+$ and $NK1.1^+$); CD69 expression profiles on these subsets were comparable between strains (data not shown). By d8-9 PI, significant pathology was observed in the lungs of SeV-infected $MDA5^{-/-}$ mice (Figure 2A), despite the fact that comparable numbers of SeV-specific CTL were generated in both strains at this time point (Figure 2B). Grossly, lungs dissected from SeV-infected $MDA5^{-/-}$ mice exhibited enhanced areas of hemorrhage relative to control lungs (data not shown). Microscopic analysis revealed epithelial cells that were notably hyperplastic with abundant micropapillary projections. Additionally, severe bronchointerstitial pneumonia was observed, with alveolar walls adjacent to affected airways thickened and congested with chronic inflammatory cell infiltrates and hyperplastic type II pneumocytes, a lung injury pattern consistent with SeV susceptibility [46,47]. In comparison, sections obtained from control mice at these later time points exhibited moderate changes to the airway epithelium and mild interstitial infiltration (Figure 2A).

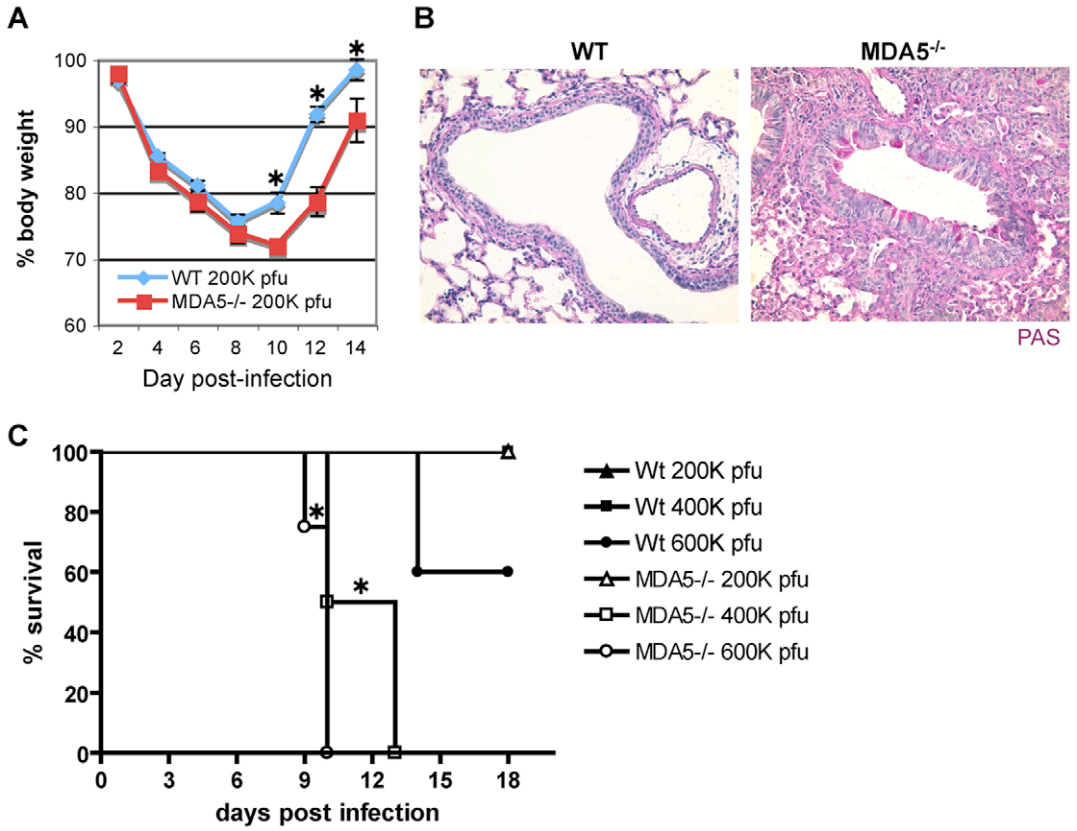

Figure 1. Infection with SeV causes increased morbidity and mortality in MDA5$^{-/-}$ mice. WT and MDA5$^{-/-}$ mice were infected with 200K pfu SeV and assessed for A) loss of body weight over the PI period and B) mucus production (PAS reactivity). C) WT and MDA5$^{-/-}$ mice were infected with 200K, 400K and 600K pfu SeV and assessed for viability. N = 4–16 mice, error bars refer to SEM, * P≤0.05.
doi:10.1371/journal.ppat.1000734.g001

MDA5$^{-/-}$ mice demonstrate increased susceptibility to SeV propagation

As susceptibility to SeV infection correlates with increased viral burden [48], we next assessed viral replication in wild type and MDA5$^{-/-}$ mice using a combined approach of real-time PCR analysis and specific staining for SeV antigens. Initially, at d2 PI, IF staining of viral antigens in lung sections appeared comparable between the two strains. By d5 PI, SeV antigens exhibited restrained expression in the airways of control mice (Figure 3A top of panel). In contrast, the bronchioles of MDA5$^{-/-}$ mice remained notably positive for SeV antigens at this time point (Figure 3A bottom of panel). More striking however, was the observation that parenchyma tissues proximal to infected airways stained conspicuously for SeV antigens in MDA5$^{-/-}$ mice at d5 PI. In SeV resistant strains of mice, SeV infection is typically restricted to the mucociliary epithelium of the conducting airways, including the trachea, bronchi and bronchioles [49,50]. Viral replication that extends to the alveolar spaces is a feature commonly seen in susceptible strains of mice [51]. Accordingly, this pattern of infection supports a role for MDA5 in controlling the replication of SeV during in vivo infection.

To confirm this finding, we measured viral RNA levels from WT and MDA5$^{-/-}$ mice infected with 200K pfu SeV using real-time PCR analysis. Assessment was made using primer/probe sets designed to amplify SeV genome (3′ untranslated region) and SeV N gene (genomic and transcript) (Figure 3B and C). Using this strategy, an approximate 5 fold increase in SeV genome copy number/*Gapdh* mRNA was detected on d5 PI, though significant differences were also observed on d2 and d8 PI. Analysis of N gene revealed ~2 fold increase in expression on days 2 and 5, though there were no significant differences by d8 PI. Thus it appears that MDA5 contributes in part to the containment of SeV replication in vivo.

Cytokine response to SeV infection is altered in MDA5$^{-/-}$ mice

Though SeV is a potent inducer of type I IFN in the mouse, functioning via several distinct pathways, it possesses several mechanisms by which it can counteract the IFN response. Despite this property, induction of IFN expression [14,52], particularly type I and II, is critical in the containment of SeV infection in vivo as underscored by the profound SeV susceptibility seen for mice deficient in STAT1$^{-/-}$ mice [53]. As MDA5 is known to induce expression of type I IFN in vitro in response to polyI:C stimulation and viral infection [17], we sought to directly assess the ability of MDA5$^{-/-}$ mice to express IFN in response to SeV infection. In this regard, WT and MDA5$^{-/-}$ mice were infected with 200K pfu SeV and subsequently assessed for cytokine expression by real-time PCR analysis over the acute period. While both strains demonstrated comparable mRNA levels at d2 PI, type I IFN expression was dramatically dampened in MDA5$^{-/-}$ mice at d5 PI (Figure 4A and B). Unexpectedly, significant decreases in expression of *Ifn-γ*, *Il-28b (Ifn-λ3)* and *Tnf-α* mRNA were also observed in the lungs of MDA5$^{-/-}$ mice compared to the WT cohort, with the most dramatic difference observed for *Il-28b* mRNA expression (Figure 4C, D and E). In contrast, *Il-1β*, and *Il-*

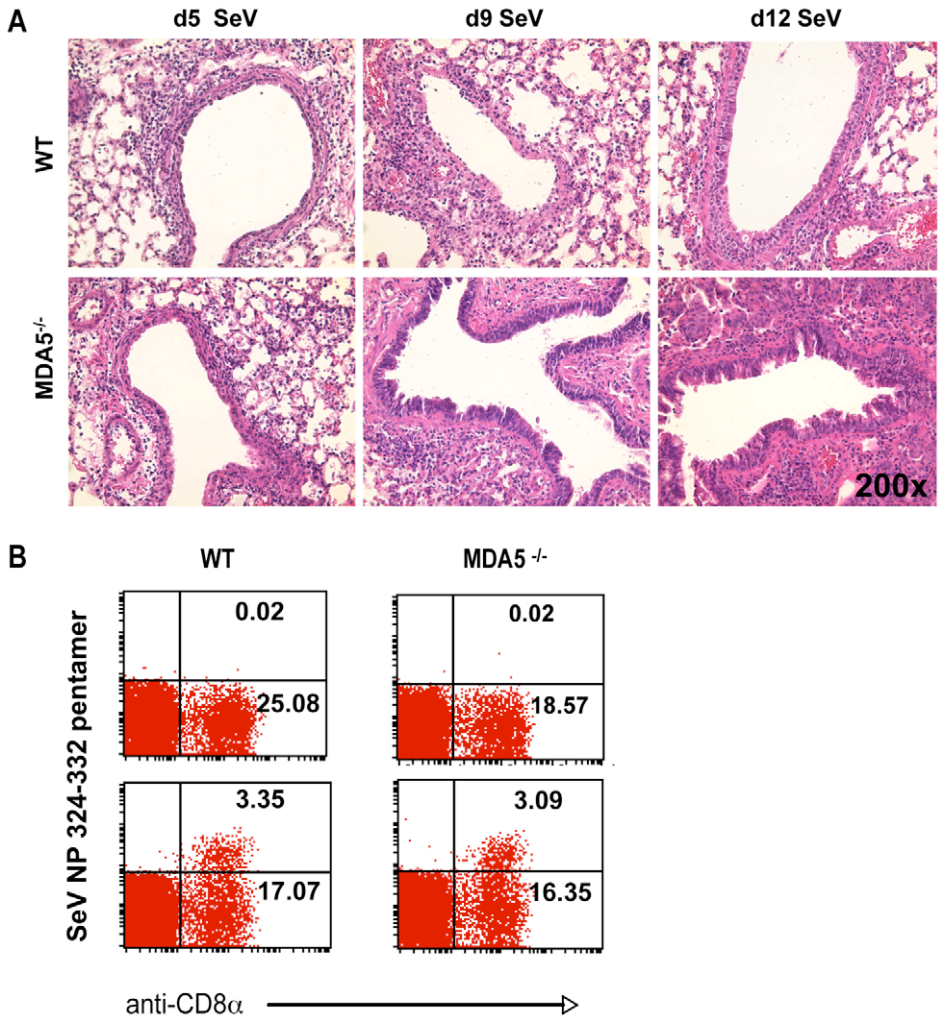

Figure 2. Increased histopathology in MDA5$^{-/-}$ mice. A) H&E micrographs of lung sections obtained from WT and MDA5$^{-/-}$ mice infected with 400K pfu SeV on d5, d9, d12 PI. B) FACS analysis of lymphocytes derived from the lungs of WT and MDA5$^{-/-}$ mice, *uninfected (top panels) and d5 post infected (bottom panels)* stained with anti-CD8 and H-2K^{b}: FAPGNYPAL pentamer.
doi:10.1371/journal.ppat.1000734.g002

10 mRNA levels were not significantly different across strains, though the levels of *Il-6* mRNA was markedly increased in MDA5$^{-/-}$ mice following infection (Figure 4F, G and H). Accordingly, MDA5 appears to control the expression of SeV-induced anti-viral cytokines, particularly type I, II and III IFNs, during the late acute period (d5 PI), but does not appear to be involved during the immediate early response. Importantly, the decrease in IFN expression coincides with expanded viral propagation in the MDA5$^{-/-}$ mice, suggesting that reduced IFN expression during this time point accounts for the corresponding increased viral burden.

Induction of IFN expression transactivates expression of a number of IFN response genes through a signal transduction cascade involving JAK/STAT activation. MDA5 and RIG-I are among the genes induced by IFN signaling in vitro [20]. To determine the expression profile of MDA5 and RIG-I in the airways of mice infected with SeV, mRNA was measured by real-time PCR analysis from whole lung homogenates obtained from WT mice infected with 200K pfu SeV. Expression of *Mda5* and *Rig-i* mRNA was significantly increased at d2 and d5 PI, though the levels began to decline by d8 PI (Figure 5A). Lastly, to determine the tissue distribution of MDA5 expression, lung sections from d5 PI mice were stained with anti-MDA5 polyclonal antibodies. Visualization of MDA5-specific staining was performed using tyramide-based amplification. IF microscopic analysis of affected airways revealed a pattern of MDA5 expression that was primarily restricted to the airway epithelium, though expression was also detected in cells of the proximal interstitum, in particular, in cells that appeared to resemble type II pneumocytes and alveolar macrophage (Figure 5B). Sections from MDA5$^{-/-}$ mice did not stain for MDA5, confirming the specificity of anti-MDA5 staining. Accordingly these findings indicate that MDA5 is induced following SeV infection and that the lack of expression in MDA5$^{-/-}$ mice accounts for the phenotype described at the later time point.

Discussion

Our understanding of innate immune factors that recognize and respond to pathogens has greatly expanded over the last decade. A major component of the RNA virus detection system in mammals involves members of the RLR family, including RIG-I, MDA5, and LGP2 [1]. Elucidating a role for the RLRs in virus-induced IFN production has been facilitated by the availability of

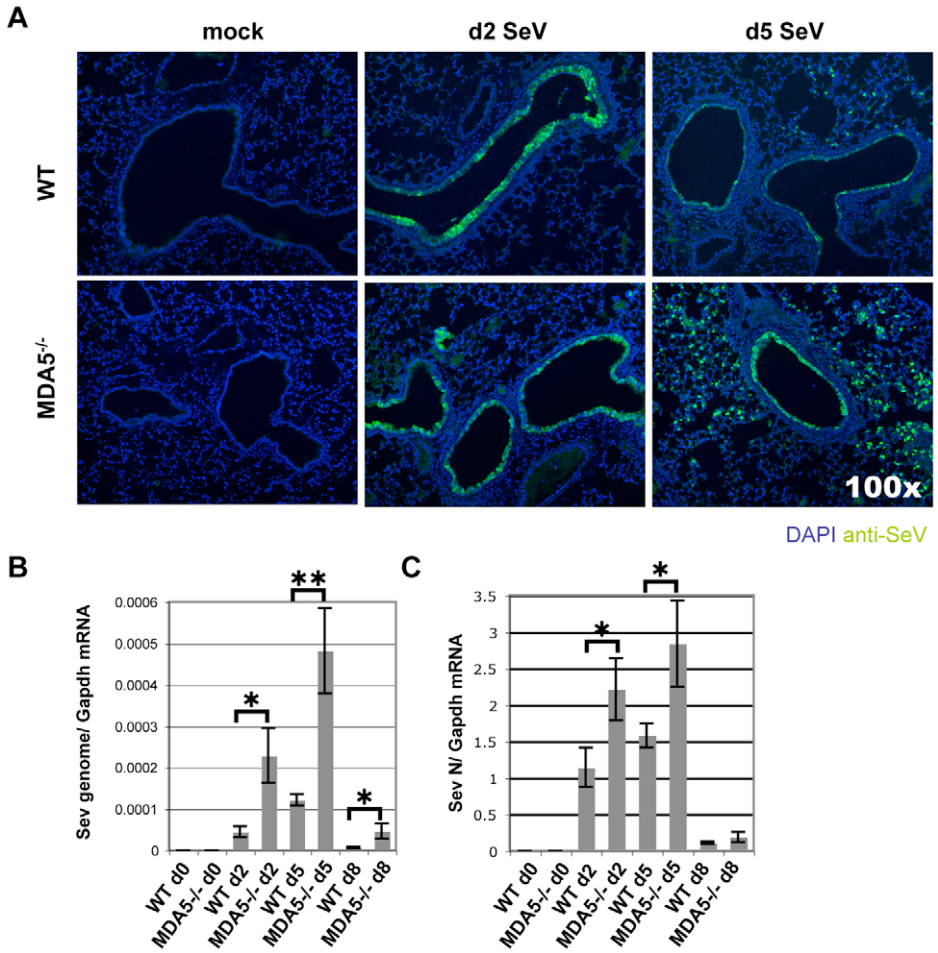

Figure 3. SeV replication is enhanced in MDA5$^{-/-}$ mice. WT and MDA5$^{-/-}$ mice infected with 200K pfu SeV were assessed for A) SeV replication by IF detection of SeV antigens and by real time PCR analysis of B) SeV genome and C) SeV N gene expression. N = 4, error bars refer to SEM, * $P<0.05$; ** $P<0.005$.
doi:10.1371/journal.ppat.1000734.g003

RIG-I$^{-/-}$ and MDA5$^{-/-}$ mice [32,33]. Initial observations using embryonic fibroblasts and bone marrow derived DCs generated from these mice revealed striking phenotypes including a failure to produce IFN in response to a wide cross-section of viruses and nucleic acids, and an inability to contain viral replication. Specifically, MDA5 was found to be the sole receptor for picornaviruses and caliciviruses ((+) ssRNA viruses) [32,33,35], whereas RIG-I was described as the receptor for (−) ssRNA viruses such as paramyxoviruses and orthomyxoviruses, as well as for (+) ssRNA viruses belonging to the *Flaviridae* family [16,33]. However, our understanding of these virus recognition systems in vivo is limited, in part because RIG-I$^{-/-}$ mice die perinatally.

The precise molecular patterns of virus replication recognized by RIG-I and MDA5 are still not fully clear. Initially, a mimic of viral dsRNA, polyI:C, was found to bind and activate RIG-I. However, ensuing research identified 5′-triphosphate-linked ssRNA as the major RIG-I inducer [27,28]. Furthermore, in vitro data obtained using knockout mice suggested in fact that MDA5, and not RIG-I, recognizes polyI:C, thereby formulating a recognition model whereby RIG-I recognizes short 5′-triphosphorylated RNAs, while MDA5 recognizes dsRNA structures irrespective of the 5′ cap [8,30–32]. However, more thorough dissection of the helicase binding function and activation process has recently determined that the picture is indeed more complex than previously thought [29,40]. In this regard, both helicases have been shown to recognize dsRNA, in a manner that is likely dependent on its length, while RIG-I demonstrates the added ability to respond to 5′-triphosphate ssRNA products. To complicate these paradigms, there is increasing evidence that viruses have evolved various properties aimed at antagonizing or degrading viral sensors. Thus, our understanding of viral recognition by the RLR helicases is evolving.

With respect to molecular sensing of paramyxovirus infection, both 5′-triphosphorylated ssRNA and long dsRNA species are likely present in SeV-infected cells, thereby implicating both MDA5 and RIG-I in the antiviral sensing process. However, in vitro studies concur that cultured embryonic fibroblasts and bone marrow-derived DC cells detect SeV RNA chiefly through RIG-I, whereas MDA5 and TLR3 are dispensable [33,34,41,54]. TLR7 and TLR8 in myeloid cells have also been shown to recognize SeV RNA in vitro as well [55]. Regardless, it cannot be excluded that in vivo, other RNA sensors, including MDA5, may contribute, at least in part, to anti-SeV responses. Indeed, a recent study by Yount et al. has demonstrated that MDA5 can detect SeV DI particles in vitro [45]. The relevancy of this recognition system in vivo is uncertain; certainly in our hands, using SeV/52, which has a limited ability to form DI particles, as per PCR-based analysis (data not shown), MDA5 appears to exert a significant effect on

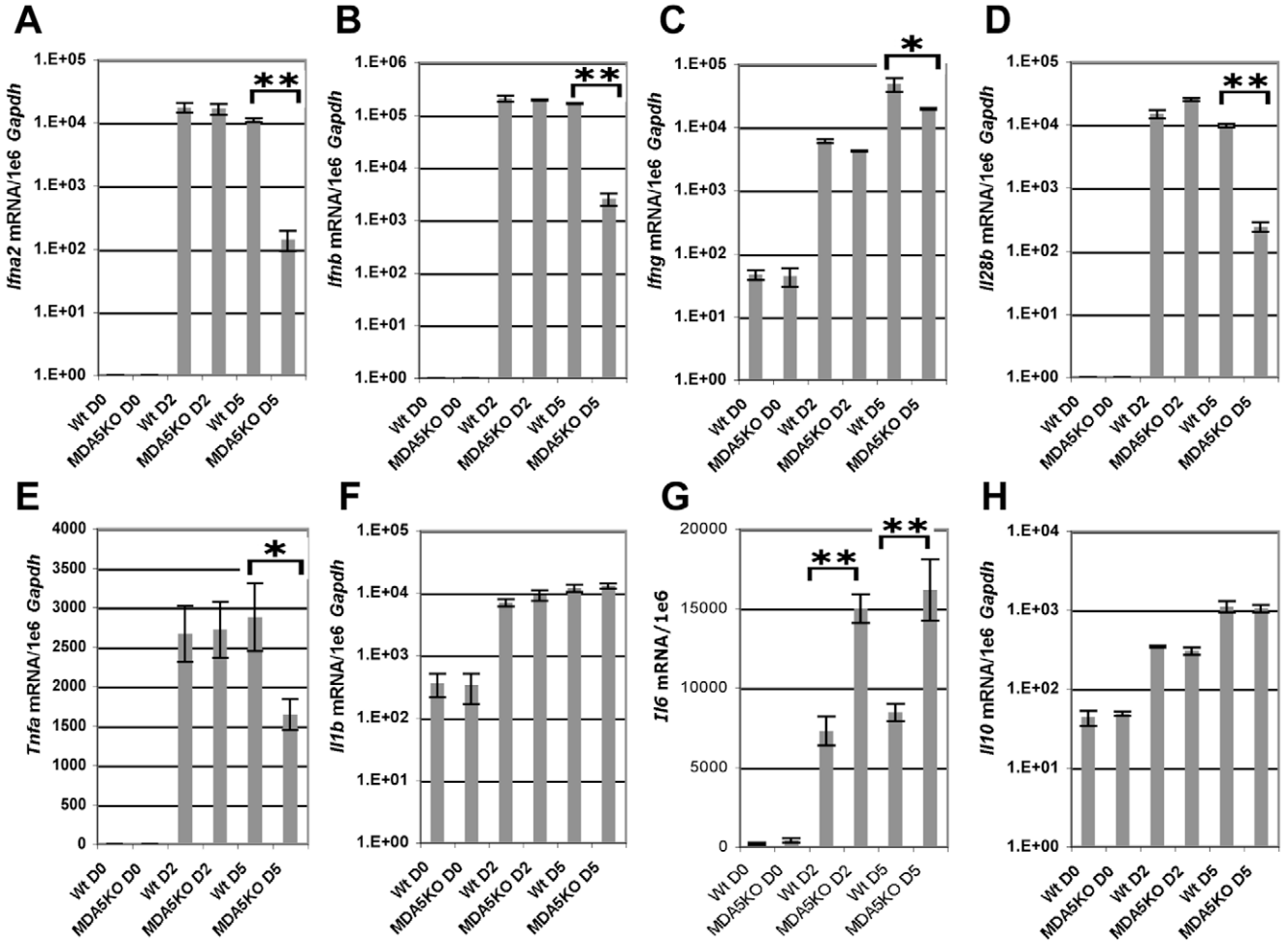

Figure 4. MDA5 is required for sustained expression of cytokines in response to SeV infection. Real time PCR analysis of whole lung homogenates obtained from WT and MDA5$^{-/-}$ mice infected with 200K pfu SeV for expression levels of A) *Ifn-α2*, B) *Ifn-β*, C) *Ifn-γ*, D) *Il-28b*, E) *Tnf-α*, F) *Il-1β*, G) *Il-6 and* H) *Il-10* mRNA. N = 4, error bars refer to SEM, * $P<0.05$, ** $P<0.00001$.
doi:10.1371/journal.ppat.1000734.g004

viral containment. Most importantly however, SeV encodes a V protein that specifically binds to and blocks MDA5 signaling in vitro [14,44]. Thus, it is possible that MDA5 does, indeed, detect SeV in vitro, but that it is functionally curtailed by the V protein in this circumstance. Interestingly, in our hands, in vivo infections using SeV with V protein deletion resulted in no real effect on mortality or type I IFN induction across strains (data not shown), likely explained by the fact that deletion of V protein in SeV markedly attenuates virulence and pathogenicty in vivo [56].

While initial characterization of MDA5-deficient cells has not supported a role for MDA5 in containment of SeV, these studies have been limited to observations made in cultured embryonic fibroblasts and in vitro-derived dendritic cells; populations which are not primary targets for SeV replication in the course of the natural infection. Rather, SeV replication mostly occurs in the airway epithelium of the conducting airways [49,50]. For these reasons, we hypothesized that SeV propagation would be sensitive to the MDA5 status of the host in the context of an in vivo infection. Indeed, the epithelial cells constitutively express MDA5 at low levels and subsequently up-regulate expression in response to SeV (Figure 5B), a finding that supports the relevance of this RNA helicase to SeV and other airborne infections. Interestingly, MDA5 deficiency did not influence the composition of the inflammatory infiltrate (data not shown), implying that the immune defect is largely restricted to the airway epithelium, the site of viral replication. This is compatible with our earlier findings using STAT-1$^{-/-}$ chimeras, wherein we observed that loss of IFN response in the stromal compartment alone accounted for the immune deficiency to SeV [53]. We therefore sought to further assess the significance of MDA5 in the control of SeV infection in vivo. In this regard we have demonstrated that MDA5 controls SeV replication and spread through induction of type I IFNs, but that this effect appears late (d5 PI), as IFN gene transcription is not impaired on d2 PI (Figure 4). It is likely that the initial IFN response is sufficient to initiate a range of immune responses, such that the late reduction in IFN transcripts results only in a 2–3 fold change in LD_{50} (Figure 1). Whether this specific IFN pattern remains true for other viruses as well remains to be tested. This surprising collapse of the host type I IFN response at d5 PI is accompanied by parallel decreases in the level of *Il-28b* and *Tnf-α* expression (Figure 4), and, curiously, decreased *Ifn-γ* transcript levels. This later observation may reflect a selective role for MDA5 in the induction of IFN-γ expression by NK cells. Lastly, the MDA5 status does not appear to influence the levels of IL-1β, or IL-10 or the ability of the host to mount a virus-specific CTL response. However, the levels of *Il-6* mRNA in whole lung

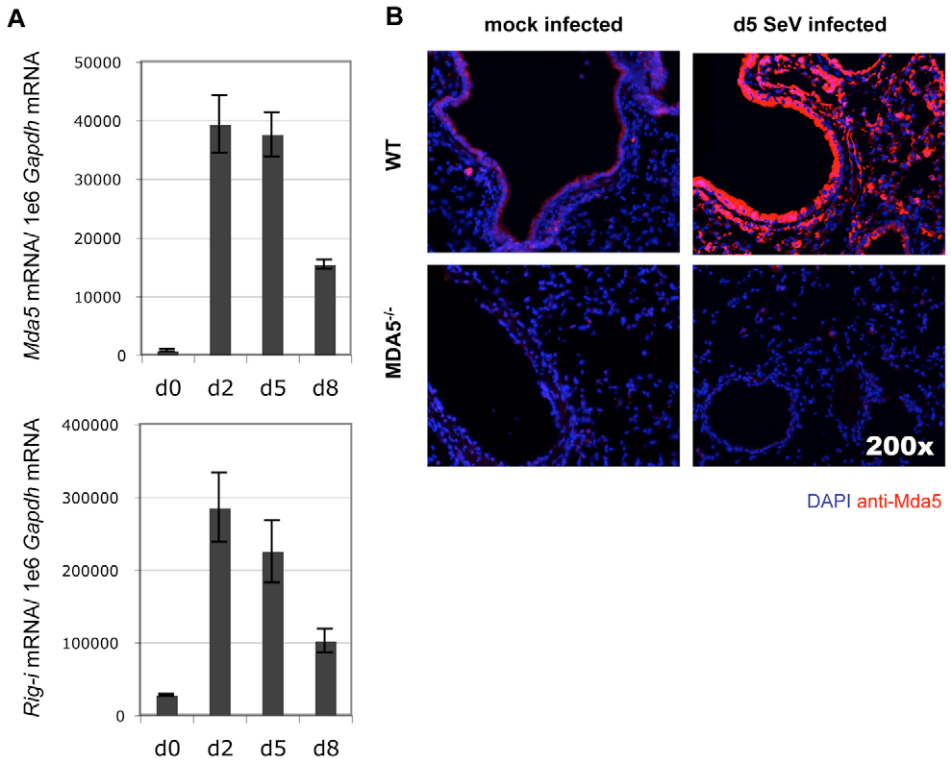

Figure 5. Infection with SeV results in induction of antiviral sensor expression. A) Analysis of *Mda5* and *Rig-I* mRNA expression in WT mice during the acute SeV infection period as determined by real-time PCR analysis. B) Micrographs taken of lung sections obtained from WT and MDA5$^{-/-}$ mice infected with 200K pfu SeV and stained for MDA5 expression. N = 4, error bars refer to SEM, * $P<0.05$.
doi:10.1371/journal.ppat.1000734.g005

homogenates derived from d2 and d5 PI MDA5$^{-/-}$ was markedly increased, suggesting the induction of compensatory mechanisms in the context of MDA5 deficiency that could potentially account for the enhanced morbidity and mortality seen in the MDA5$^{-/-}$ mice.

An additional concern raised by these data is the relative contribution of MDA5 and RIG-I in the response to virus. In light of the existing literature [33,40], it seems likely that RIG-I is responsible for the normal IFN response to SeV early in the infection. Indeed, as depicted in Figure 5A, RIG-I is strongly induced early on during infection. Why the later IFN response depends on MDA5 is not known. MDA5 is encoded by an IFN-upregulated transcript, and it remains possible that it is the accumulation of MDA5 that allows for the subsequent MDA5-dependent IFN response on d5 PI. Yet other IFN-induced genes, notably RIG-I, are also upregulated by IFN, which should provide additional antiviral protection in vivo. Interestingly, SeV encodes a nested set of C proteins that have been shown to impede IFN signaling through direct inhibition of STAT signaling [41,42] and which are also known to strongly antagonize RIG-I function [41]. Furthermore, SeV-V proteins have been shown to have direct inhibitory effects on both MDA5 and RIG-I signaling [41,44]. Thus it remains possible that the effects of SeV V and C proteins have an accumulative effect on RIG-I function that essentially overwhelms this sensor at d5 PI, and that in this context, MDA5 plays an essential role in containment of SeV. Since assessment of the relative contribution of RIG-I and MDA5 in containment of SeV infection in vivo is not possible, a possible next step in assessing the importance of MDA5 function would involve assessment in MDA5$^{-/-}$ and IPS-1$^{-/-}$ strains.

We envision several possibilities that could potentially explain this dramatic effect of MDA5. The first is that, in the absence of MDA5, the balance between virus replication and the IFN response is disrupted sufficiently, such that by d5 PI, virus replication has overwhelmed the response in a qualitative fashion –presumably through direct cytotoxic effects or via the overproduction of immunosuppressive C proteins. This possibility is supported by the fact that SeV is replicating to higher levels in the MDA5$^{-/-}$ lung already by d2 PI (Figure 3B). Indeed, in support of this hypothesis, we observe a striking increase in SeV replication that spreads extensively into the interstitium of MDA5$^{-/-}$ lungs compared to controls. Another possible explanation, which we have not assessed, is an apoptotic response potentially mediated by MDA5. In this scenario, MDA5 would instruct or sensitize infected cells to commit suicide so as to shut down viral replication in infected cells. Indeed, ectopic expression of MDA5 in a melanoma cell line has been shown to inhibit colony formation, presumably through induction of apoptosis [20], and IPS-1 overexpression induces cell death, as well [57]. In fact, SeV-dependent apoptotic signaling requires IRF3 [58]. In the case of MDA5 deficiency, loss of pro-apoptotic activity could lead to a robust increase in viral replication and enhanced IFN blockade through overexpression of SeV C proteins. This possibility is favored by the fact that, despite a normal IFN response on d2 PI (Figure 4), the virus is found to be replicating at higher titers (Figure 3B).

It seems likely that the inability of the MDA5$^{-/-}$ animals to sustain an IFN response leads to increased viral replication and dissemination on d5 PI, thus causing significantly higher morbidity and mortality in the knockout cohort (Figure 1). It is important to note, however, that the effects of MDA5 deficiency on SeV

replication are much milder than expected if MDA5 were the sole target of the V protein. Indeed, SeV V mutants (SeV-ΔV) are severely attenuated; replication is demonstrably abrogated in the lungs by d2 PI [56]. IRF3 deficiency of the host restores SeV-ΔV pathogenicity, suggesting that the mutant virus acts by blocking IRF3 signaling [59]. Yet disease caused by SeV in MDA5$^{-/-}$ mice is milder than the disease seen in the IRF3$^{-/-}$ animals. Consequently, we believe that the V protein must have additional targets besides MDA5. In this regard, it has recently been demonstrated that *Lgp2* encodes a helicase epitope that is akin to the MDA5 helicase, the portion of MDA5 that binds paramyxovirus V proteins [60], thereby suggesting that LGP2 may be an additional V protein target. In this case, a MDA5-LGP2 double knockout mouse may potentially phenocopy the IRF3 mutation in its response to SeV infection.

Taken together, our findings demonstrate that MDA5 significantly contributes to the response to paramyxovirus and constitute the first in vivo demonstration of MDA5 activity against a negative-strand virus. As such, it appears likely that MDA5 has a wider specificity as a viral nucleic acid receptor than initially believed, and that the initial clear-cut cases of either MDA5 or RIG-I being the sole receptor for a given virus will prove to be exceptions rather than rules when studied in the context of in vivo infections.

Materials and Methods

Mouse generation, maintenance and infection

Control C57BL/6J (B6) mice used in these experiments were purchased from JAX. MDA5$^{-/-}$ mice [32] were backcrossed onto the B6 background to 99.9% congenicity. For in vivo SeV infection, Sendai/52 Fushimi strain was instilled intranasally into deeply anesthetized mice and at the indicated time points, mice were humanly sacrificed for harvest of lung tissue. Virus was purchased from the ATCC and subject to two rounds of in vitro plaque purification in Vero cells to eliminate the presence of DI particles. A clone thus identified was then subject to a single round of amplification in embryonated chicken eggs following inoculation of ~1000 PFU. 24–36 hr post inoculation, SeV was isolated from the allantoic fluids and diluted in phosphate-buffered solution to generate a viral stock that was subsequently characterized on the basis of in vivo infectious properties. Calculation of PFU was performed by standard plaque assay using either Vero E6 cells or LLC-MK2 cells. Importantly, propagation under these conditions does not favor the formation of DI particles, a process that occurs most frequently when virus is repeatedly passaged at high MOI. Indeed, PCR analysis of stock virus indicated the absence of DI genomes. The methods for mice use and care were approved by the Washington University Animal Studies Committee and are in accordance with NIH guidelines.

FACS

Single cell lung suspensions were made from minced lung tissue subjected to collagenase/hyaluronidase/DNAse I digestion. Staining of surface markers was performed using FcR block and fluorochrome-conjugated mAbs. To immunophenotype the immune infiltrate, specific combinations of mAbs were chosen which discern granulocytes (Ly6G$^+$), macrophages (F4/80$^+$), cDC (CD11c$^+$F4/80$^-$Siglec-H$^-$), pDC (Siglec-H$^+$ CD11c^{mid}), NK cells (NK1.1$^+$NKp46$^+$), T cells (CD3$^+$CD4$^{+/-}$CD8$^{+/-}$) and B cells (CD19$^+$). SeV-specific PE-labeled pentamer K^b:FAPGNYPAL (NP 324-332) was purchased from Proimmune; cells were stained with CD8 and counterstained with propidium iodide, F4/80 and CD19 to eliminate background. Activation status was determined using specific mAbs for MHC-II, NKG2D and CD69. Samples were acquired on a FACScalibur (BD Biosciences) and analyzed using Cellquest software.

Analysis of mRNA and virus-specific RNA

RNA was purified from lung homogenate using Trizol Reagent (Invitrogen). RNA was treated with RNAse-free DNAse I (Ambion) to eliminate genomic DNA. RNA was converted to cDNA using the High-Capacity cDNA Archive kit (Applied Biosystems). Target mRNA and viral RNAs were quantified by real-time PCR using specific fluorogenic probes and primers and the Fast Universal PCR Master Mix system (Applied Biosystems). Primer sets and probes for mouse *Ifn-α2* (Mm00833961_s1), *Ifn-β* (Mm00439552_s1), *Ifn-γ* (Mm00801778-m1), *Il-28b* (Mm00663660_g1), *Tnf-α* (Mm00443259_g1), *Mda5* (Mm00459183_m1), *Il-1β* (Mm00434227_g1), *Il-6* (Mm00446190_m1), *Il-10* (Mm00439616_m1) mRNA and SeV genome and *Gapdh* mRNA were purchased from Applied Biosystems. Samples were assayed on the 7500 Fast Real-Time PCR System and analyzed using the 7500 Fast System Software (Applied Biosystems). Levels of specific gene expression were standardized to *Gapdh* mRNA expression levels.

Histology

Lungs were perfused and fixed with 4% paraformaldehyde. Tissue was embedded in paraffin, cut into 5 um sections and adhered to charged slides. Sections were deparaffinized in Citrosolv (Fisherbrand), hydrated, and in the case of IF-microscopy, treated to heat-activated antigen unmasking solution (Vector Laboratories, Inc). H&E and PAS sections were visualized by brightfield microscopy. Expression analysis was performed by IF using chicken polyclonal anti-SeV (Jackson ImmunoResearch Laboratories, Inc) and rabbit polyclonal anti-mouse MDA5 (Axxora Life Sciences, Inc). Biotinylated secondary antibodies were purchased from Vector Laboratories, Inc). SeV and MDA5 expression was visualized using tyramide-based signal amplification with Alexa Fluor 488 or 594 fluorochromes (Invitrogen). Slides were counterstained with DAPI mounting media (Vector Laboratories, Inc). Microscopy was performed using an Olympus BX51 microscope.

Statistical analyses

Real-time PCR data was analyzed using an unpaired Student's t-test. If variances were unequal, Welch's correction was applied. Charted values represent mean ± SEM. Survival statistics were determined using by Kaplan-Meier analysis of paired cohorts. P values below 0.05 were regarded as being significant for all analyses. Experiments were repeated a minimum of three times.

Author Contributions

Conceived and designed the experiments: M. Holtzman, M. Colonna. Performed the experiments: L. Benoit, C. Song, M. Cella. Analyzed the data: L. Gitlin, L. Benoit, M. Holtzman. Contributed reagents/materials/analysis tools: L. Gitlin, M. Cella, S. Gilfillan. Wrote the paper: L. Gitlin, L. Benoit.

References

1. Kawai T, Akira S (2008) Toll-like Receptor and RIG-1-like Receptor Signaling. Annals of the New York Academy of Sciences 1143: 1–20.

2. Kotenko SV, Pestka S (2000) Jak-Stat signal transduction pathway through the eyes of cytokine class II receptor complexes. Oncogene 19: 2557–2565.

3. Schindler C, Darnell JE (1995) Transcriptional Responses to Polypeptide Ligands: The JAK-STAT Pathway. Annual Review of Biochemistry 64: 621–652.
4. de Veer MJ, Holko M, Frevel M, Walker E, Der S, et al. (2001) Functional classification of interferon-stimulated genes identified using microarrays. J Leukoc Biol 69: 912–920.
5. Stetson DB, Medzhitov R (2006) Type I Interferons in Host Defense. Immunity 25: 373–381.
6. Braun D, Caramalho I, Demengeot J (2002) IFN-{alpha}/{beta} enhances BCR-dependent B cell responses. Int Immunol 14: 411–419.
7. Tough DF (2004) Type I interferon as a link between innate and adaptive immunity through dendritic cell stimulation. Leukemia & Lymphoma 45: 257–264.
8. Saito T, Hirai R, Loo Y-M, Owen D, Johnson CL, et al. (2007) Regulation of innate antiviral defenses through a shared repressor domain in RIG-I and LGP2. Proceedings of the National Academy of Sciences 104: 582–587.
9. Iwasaki A, Medzhitov R (2004) Toll-like receptor control of the adaptive immune responses. Nat Immunol 5: 987–995.
10. Alexopoulou L, Holt AC, Medzhitov R, Flavell RA (2001) Recognition of double-stranded RNA and activation of NF-kappaB by Toll-like receptor 3. Nature 413: 732–738.
11. Diebold SS, Kaisho T, Hemmi H, Akira S, Reis e Sousa C (2004) Innate antiviral responses by means of TLR7-mediated recognition of single-stranded RNA.[see comment]. Science 303: 1529–1531.
12. Heil F, Hemmi H, Hochrein H, Ampenberger F, Kirschning C, et al. (2004) Species-specific recognition of single-stranded RNA via toll-like receptor 7 and 8.[see comment]. Science 303: 1526–1529.
13. Bauer S, Kirschning CJ, HÃ¤cker H, Redecke V, Hausmann S, et al. (2001) Human TLR9 confers responsiveness to bacterial DNA via species-specific CpG motif recognition. Proceedings of the National Academy of Sciences of the United States of America 98: 9237–9242.
14. Andrejeva J, Childs KS, Young DF, Carlos TS, Stock N, et al. (2004) The V proteins of paramyxoviruses bind the IFN-inducible RNA helicase, mda-5, and inhibit its activation of the IFN-beta promoter. Proceedings of the National Academy of Sciences of the United States of America 101: 17264–17269.
15. Rothenfusser S, Goutagny N, DiPerna G, Gong M, Monks BG, et al. (2005) The RNA helicase Lgp2 inhibits TLR-independent sensing of viral replication by retinoic acid-inducible gene-I. Journal of Immunology 175: 5260–5268.
16. Sumpter R Jr, Loo YM, Foy E, Li K, Yoneyama M, et al. (2005) Regulating intracellular antiviral defense and permissiveness to hepatitis C virus RNA replication through a cellular RNA helicase, RIG-I. Journal of Virology 79: 2689–2699.
17. Yoneyama M, Kikuchi M, Matsumoto K, Imaizumi T, Miyagishi M, et al. (2005) Shared and unique functions of the DExD/H-box helicases RIG-I, MDA5, and LGP2 in antiviral innate immunity. Journal of Immunology 175: 2851–2858.
18. Yoneyama M, Kikuchi M, Natsukawa T, Shinobu N, Imaizumi T, et al. (2004) The RNA helicase RIG-I has an essential function in double-stranded RNA-induced innate antiviral responses.[see comment]. Nature Immunology 5: 730–737.
19. Komuro A, Horvath CM (2006) RNA and Virus-Independent Inhibition of Antiviral Signaling by RNA Helicase LGP2. Journal of Virology.
20. Kang DC, Gopalkrishnan RV, Wu Q, Jankowsky E, Pyle AM, et al. (2002) mda-5: An interferon-inducible putative RNA helicase with double-stranded RNA-dependent ATPase activity and melanoma growth-suppressive properties. Proceedings of the National Academy of Sciences of the United States of America 99: 637–642.
21. Kovacsovics M, Martinon F, Micheau O, Bodmer JL, Hofmann K, et al. (2002) Overexpression of Helicard, a CARD-containing helicase cleaved during apoptosis, accelerates DNA degradation.[erratum appears in Curr Biol. 2002 Sep 17;12(18):1633.]. Current Biology 12: 838–843.
22. Venkataraman T, Valdes M, Elsby R, Kakuta S, Caceres G, et al. (2007) Loss of DExD/H Box RNA Helicase LGP2 Manifests Disparate Antiviral Responses. J Immunol 178: 6444–6455.
23. Kawai T, Takahashi K, Sato S, Coban C, Kumar H, et al. (2005) IPS-1, an adaptor triggering RIG-I- and Mda5-mediated type I interferon induction.[see comment]. Nature Immunology 6: 981–988.
24. Meylan E, Curran J, Hofmann K, Moradpour D, Binder M, et al. (2005) Cardif is an adaptor protein in the RIG-I antiviral pathway and is targeted by hepatitis C virus. Nature 437: 1167–1172.
25. Seth RB, Sun L, Ea CK, Chen ZJ (2005) Identification and characterization of MAVS, a mitochondrial antiviral signaling protein that activates NF-kappaB and IRF 3.[see comment]. Cell 122: 669–682.
26. Xu LG, Wang YY, Han KJ, Li LY, Zhai Z, et al. (2005) VISA is an adapter protein required for virus-triggered IFN-beta signaling. Molecular Cell 19: 727–740.
27. Hornung V, Ellegast J, Kim S, Brzozka K, Jung A, et al. (2006) 5′-Triphosphate RNA Is the Ligand for RIG-I. Science 314: 994–997.
28. Pichlmair A, Schulz O, Tan CP, Naslund TI, Liljestrom P, et al. (2006) RIG-I-Mediated Antiviral Responses to Single-Stranded RNA Bearing 5′-Phosphates. Science 314: 997–1001.
29. Kato H, Takeuchi O, Mikamo-Satoh E, Hirai R, Kawai T, et al. (2008) Length-dependent recognition of double-stranded ribonucleic acids by retinoic acid-inducible gene-I and melanoma differentiation-associated gene 5. J Exp Med 205: 1601–1610.
30. Saito T, Gale M Jr (2008) Differential recognition of double-stranded RNA by RIG-I-like receptors in antiviral immunity. J Exp Med 205: 1523–1527.
31. Saito T, Owen DM, Jiang F, Marcotrigiano J, Gale Jr M (2008) Innate immunity induced by composition-dependent RIG-I recognition of hepatitis C virus RNA. Nature 454: 523–527.
32. Gitlin L, Barchet W, Gilfillan S, Cella M, Beutler B, et al. (2006) Essential role of mda-5 in type I IFN responses to polyriboinosinic:polyribocytidylic acid and encephalomyocarditis picornavirus. Proceedings of the National Academy of Sciences of the United States of America 103: 8459–8464.
33. Kato H, Takeuchi O, Sato S, Yoneyama M, Yamamoto M, et al. (2006) Differential roles of MDA5 and RIG-I helicases in the recognition of RNA viruses. Nature 441: 101–105.
34. Loo Y-M, Fornek J, Crochet N, Bajwa G, Perwitasari O, et al. (2008) Distinct RIG-I and MDA5 Signaling by RNA Viruses in Innate Immunity. J Virol 82: 335–345.
35. McCartney SA, Thackray LB, Gitlin L, Gilfillan S, Virgin Iv HW, et al. (2008) MDA-5 Recognition of a Murine Norovirus. PLoS Pathog 4: e1000108. doi:10.1371/journal.ppat.1000108.
36. Fredericksen BL, Keller BC, Fornek J, Katze MG, Gale M Jr (2008) Establishment and Maintenance of the Innate Antiviral Response to West Nile Virus Involves both RIG-I and MDA5 Signaling through IPS-1. J Virol 82: 609–616.
37. Collins PL, Chanock RM, McIntosh K (1996) Parainfluenza Viruses. In: Fields, ed. Fields Virology. Philadelphia: Lippincott-Raven.
38. Collins PL, Chanock RM, McIntosh K (1996) Respiratory Syncytial Virus. Fields Virology. Philadelphia: Lippincott-Raven.
39. Walter MJ, Kajiwara N, Karanja P, Castro M, Holtzman MJ (2001) Interleukin 12 p40 Production by Barrier Epithelial Cells during Airway Inflammation. J Exp Med 193: 339–352.
40. Hausmann S, Marq J-B, Tapparel C, Kolakofsky D, Garcin D (2008) RIG-I and dsRNA-Induced IFNÎ² Activation. PLoS ONE 3: e3965. doi:10.1371/journal.pone.0003965.
41. Strahle L, Marq J-B, Brini A, Hausmann S, Kolakofsky D, et al. (2007) Activation of the Beta Interferon Promoter by Unnatural Sendai Virus Infection Requires RIG-I and Is Inhibited by Viral C Proteins. J Virol 81: 12227–12237.
42. Garcin D, Latorre P, Kolakofsky D (1999) Sendai Virus C Proteins Counteract the Interferon-Mediated Induction of an Antiviral State. J Virol 73: 6559–6565.
43. Gotoh B, Takeuchi K, Komatsu T, Yokoo J, Kimura Y, et al. (1999) Knockout of the Sendai virus C gene eliminates the viral ability to prevent the interferon-[alpha]/[beta]-mediated responses. FEBS Letters 459: 205–210.
44. Childs K, Stock N, Ross C, Andrejeva J, Hilton L, et al. (2007) mda-5, but not RIG-I, is a common target for paramyxovirus V proteins. Virology 359: 190–200.
45. Yount JS, Gitlin L, Moran TM, Lopez CB (2008) MDA5 Participates in the Detection of Paramyxovirus Infection and Is Essential for the Early Activation of Dendritic Cells in Response to Sendai Virus Defective Interfering Particles. J Immunol 180: 4910–4918.
46. Parker JC, Whiteman MD, Richter CB (1978) Susceptibility of inbred and outbred mouse strains to Sendai virus and prevalence of infection in laboratory rodents. Infect Immun 19: 123–130.
47. Itoh T, Iwai H, Ueda K (1991) Comparative lung pathology of inbred strain of mice resistant and susceptible to Sendai virus infection. Journal of Veterinary Medical Science 53: 275–279.
48. Mo XY, Sarawar SR, Doherty PC (1995) Induction of cytokines in mice with parainfluenza pneumonia. J Virol 69: 1288–1291.
49. Blandford G, Heath RB (1972) Studies on the immune response and pathogenesis of Sendai virus infection of mice. I. The fate of viral antigens. Immunology 22: 637–649.
50. Degré M, Midtvedt T (1971) Respiratory infection with parainfluenza 1, Sendai virus in gnotobiotic and conventional mice. Acta pathologica et microbiologica Scandinavica Section B: Microbiology and immunology 79: 123–124.
51. Brownstein DGSA, Johnson EA (1981) Sendai virus infection in genetically resistant and susceptible mice. The American journal of pathology 105: 156–163.
52. Takeuchi K, Komatsu T, Yokoo J, Kato A, Shioda T, et al. (2001) Sendai virus C protein physically associates with Stat1. Genes to Cells 6: 545–557.
53. Shornick LP, Wells AG, Zhang Y, Patel AC, Huang G, et al. (2008) Airway Epithelial versus Immune Cell Stat1 Function for Innate Defense against Respiratory Viral Infection. J Immunol 180: 3319–3328.
54. Lopez CB, Moltedo B, Alexopoulou L, Bonifaz L, Flavell RA, et al. (2004) TLR-Independent Induction of Dendritic Cell Maturation and Adaptive Immunity by Negative-Strand RNA Viruses. J Immunol 173: 6882–6889.
55. Melchjorsen J, Jensen SB, Malmgaard L, Rasmussen SB, Weber F, et al. (2005) Activation of innate defense against a paramyxovirus is mediated by RIG-I and TLR7 and TLR8 in a cell-type-specific manner. Journal of Virology 79: 12944–12951.
56. Kato A, Kiyotani K, Sakai Y, Yoshida T, Nagai Y (1997) The paramyxovirus, Sendai virus, V protein encodes a luxury function required for viral pathogenesis. EMBO (European Molecular Biology Organization) Journal 16: 578–587.

57. Lei Y, Moore CB, Liesman RM, O'Connor BP, Bergstralh DT, et al. (2009) MAVS-Mediated Apoptosis and Its Inhibition by Viral Proteins. PLoS ONE 4: e5466. doi:10.1371/journal.pone.0005466.
58. Peters K, Chattopadhyay S, Sen GC (2008) IRF-3 Activation by Sendai Virus Infection Is Required for Cellular Apoptosis and Avoidance of Persistence. J Virol 82: 3500–3508.
59. Kiyotani K, Sakaguchi T, Kato A, Nagai Y, Yoshida T (2007) Paramyxovirus Sendai virus V protein counteracts innate virus clearance through IRF-3 activation, but not via interferon, in mice. Virology 359: 82–91.
60. Parisien J-P, Bamming D, Komuro A, Ramachandran A, Rodriguez JJ, et al. (2009) A Shared Interface Mediates Paramyxovirus Interference with Antiviral RNA Helicases MDA5 and LGP2. J Virol: JVI.00153–00109.

Atg9a controls dsDNA-driven dynamic translocation of STING and the innate immune response

Tatsuya Saitoh[a,b,1], Naonobu Fujita[c,1], Takuya Hayashi[c], Keigo Takahara[a,b], Takashi Satoh[a,b], Hanna Lee[a,b,d], Kohichi Matsunaga[c], Shun Kageyama[c], Hiroko Omori[c], Takeshi Noda[c], Naoki Yamamoto[e], Taro Kawai[a,b], Ken Ishii[a,f], Osamu Takeuchi[a,b], Tamotsu Yoshimori[c], and Shizuo Akira[a,b,2]

[a]Laboratory of Host Defense, WPI Immunology Frontier Research Center, Osaka University, 3-1 Yamada-oka, Suita, Osaka 565-0871, Japan; [b]Department of Host Defense, [c]Department of Cellular Regulation, and [f]Department of Molecular Protozoology, Research Institute for Microbial Diseases, Osaka University, 3-1 Yamada-oka, Suita, Osaka 565-0871, Japan; [d]National Research Laboratory of Defense Proteins, College of Pharmacy, Pusan National University, Busan 609-735, Korea; and [e]AIDS Research Center, National Institute of Infectious Diseases, Toyama 1-23-1, Shinjuku-ku, Tokyo, Japan

Contributed by Shizuo Akira, October 1, 2009 (sent for review September 16, 2009)

Microbial nucleic acids are critical for the induction of innate immune responses, a host defense mechanism against infection by microbes. Recent studies have indicated that double-stranded DNA (dsDNA) induces potent innate immune responses via the induction of type I IFN (IFN) and IFN-inducible genes. However, the regulatory mechanisms underlying dsDNA-triggered signaling are not fully understood. Here we show that the translocation and assembly of the essential signal transducers, stimulator of IFN genes (STING) and TANK-binding kinase 1 (TBK1), are required for dsDNA-triggered innate immune responses. After sensing dsDNA, STING moves from the endoplasmic reticulum (ER) to the Golgi apparatus and finally reaches the cytoplasmic punctate structures to assemble with TBK1. The addition of an ER-retention signal to the C terminus of STING dampens its ability to induce antiviral responses. We also show that STING co-localizes with the autophagy proteins, microtubule-associated protein 1 light chain 3 (LC3) and autophagy-related gene 9a (Atg9a), after dsDNA stimulation. The loss of Atg9a, but not that of another autophagy-related gene (Atg7), greatly enhances the assembly of STING and TBK1 by dsDNA, leading to aberrant activation of the innate immune response. Hence Atg9a functions as a regulator of innate immunity following dsDNA stimulation as well as an essential autophagy protein. These results demonstrate that dynamic membrane traffic mediates the sequential translocation and assembly of STING, both of which are essential processes required for maximal activation of the innate immune response triggered by dsDNA.

autophagy-related gene | double-stranded DNA | interferon | membrane traffic

Innate immunity is initiated following the recognition of pathogen-associated molecular patterns and functions as a first line of host defense against infectious agents (1–3). Increasing evidence indicates that pattern recognition receptors, such as Toll-like receptors and RIG-like helicases, detect microbial nucleic acids and mediate innate immune responses (1–3). However, the system responsible for double-stranded DNA (dsDNA)-induced innate immune responses, although extensively analyzed, is still unclear. Microbial dsDNA derived from bacteria and DNA viruses, as well as synthetic dsDNA, induce both type I IFN (IFN) production and other pro-inflammatory cytokines, such as interleukin IL-1β and IL-6 (1–9). It is also known that undigested host genomic DNA accumulated in phagocytes can also induce aberrant activation of the immune response (10, 11). These findings clearly indicate that analysis of the dsDNA-induced immune response is important to understand the mechanism underlying both anti-microbial responses and the development of autoimmune disease. While absent in melanoma (AIM) 2 has been identified as a cytoplasmic dsDNA sensor required for activation of inflammasome, a caspase-1-containing complex responsible for the production of IL-1β, the sensor(s) responsible for the production of type I IFN and IFN-inducible genes by dsDNA have not yet been identified (10–11). We and others have shown that IFN regulatory factor (IRF)-3 (a transcription factor for type I IFN and IFN-inducible genes) and TANK-binding kinase (TBK) 1 (an IRF3 kinase) both play critical roles in the innate immune response initiated by dsDNA (1–7). Stimulator of IFN genes (STING), which is also called MPYS/MITA/ERIS, has recently been shown to be a multispanning membrane protein and a mediator of dsDNA-induced type I IFN production, although the mechanism responsible for the regulation of dsDNA-induced innate immune responses by STING is not known (12–15). Here we attempted to demonstrate the mechanism underlying the dsDNA-triggered innate immune response by visualization of STING translocation.

Results

STING Assembles with TBK1 After dsDNA Stimulation. We first examined the localization of STING and TBK1 both before and after dsDNA stimulation. Although previous studies have indicated the importance of STING in the innate immune response, subcellular localization of this protein, in either the ER or in mitochondria, has been controversially reported (12–15). Hence, we decided to re-examine the localization of STING in unstimulated cells. We avoided using plasmid transient transfection methods to examine the localization of STING because the plasmid itself is a dsDNA and has been shown to induce immune responses. Our results show that STING localizes to the ER, but not to mitochondria, in unstimulated MEFs (Fig. 1*A* and Fig. S1*A*). Following dsDNA stimulation, STING rapidly translocates from the ER to the Golgi apparatus and finally assembles with TBK1 in cytoplasmic punctate structures where p62/Sequestosome 1, an aggregate marker, forms puncta (Fig. 1 *B* and *C* and Fig. S1*B*) (16). STING does not localize to endosomes, lysosomes or peroxisomes (Fig. S1 *C*–*F*). Even in MEFs lacking both TBK1 and IκB kinase (IKK)-*i*, STING forms puncta following dsDNA stimulation, indicating that the translocation of STING is independent of activation of downstream regulators (Fig. S2). Translocation of STING is specifically driven by dsDNA, such as poly (dA-dT), poly (dG-dC) and bacterial DNA, since localization of STING is not altered following stimulation with ssDNA, dsRNA, LPS, or IFNβ (Fig. S3*A*). We also found that puncta formation by TBK1 is also specifically induced by dsDNA, but not by dsRNA (Fig. S3*B*). These results indicate that

Author contributions: T.N., T.Y., and S.A. designed research; T. Saitoh, N.F., T.H., K.T., T. Satoh, H.L., H.O., T.K., K.I., and O.T. performed research; K.M., S.K., and N.Y. contributed new reagents/analytic tools; and S.A. wrote the paper.

The authors declare no conflict of interest.

[1]T. Saitoh and N.F. contributed equally to this work.

[2]To whom correspondence should be addressed. E-mail: sakira@biken.osaka-u.ac.jp.

This article contains supporting information online at www.pnas.org/cgi/content/full/0911267106/DCSupplemental.

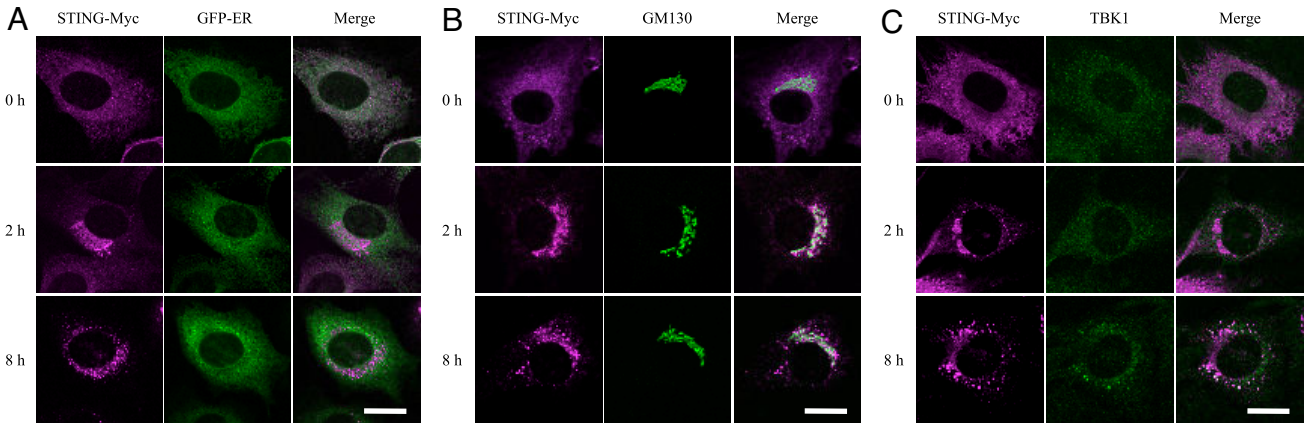

Fig. 1. Double-stranded DNA triggers the assembly of STING and TBK1. Wild-type MEFs stably expressing STING-Myc were transfected with poly (dA-dT) (1 μg/mL) for the indicated periods. The localization of STING and the indicated proteins was observed by confocal laser scanning microscopy. (Scale bars, 20 μm.)

the assembly of STING and TBK1 in cytoplasmic punctate structures is specifically driven by dsDNA stimulation.

The translocation of STING in response to dsDNA prompted us to examine whether this translocation is required for mediation of the signaling pathway. It is well known that proteins which have ER-retention signal peptides on their C terminus localize to the ER (17). We found that the addition of 'KDEL' signal peptides, but not 'KKMP' signal peptides, to the C terminus of STING reduces its ability to induce IFN-stimulation responsive element (ISRE)-dependent transcription (Fig. 2*A*). Consistent with this result, the culture supernatant from 293 cells transfected with wild-type STING, but not that of the cells transfected with STING-KDEL, suppresses replication of Herpes simplex virus (HSV)-1 (Fig. 2*B*). These results indicate that translocation of STING is necessary for activation of downstream events.

STING Colocalizes with Autophagy-Related Proteins After dsDNA Stimulation. Next we attempted to analyze the cytoplasmic punctate structures of STING induced by dsDNA. As shown in Fig. S1*B*, p62, which is selectively degraded by autophagy, co-localizes with STING after dsDNA-stimulation, suggesting regulation of the response by autophagy, a bulk degradation system that delivers cytoplasmic constituents into lysosomes (16, 18–21). Autophagy-related proteins function as essential components of the membrane traffic system required for autophagy and are critical for the degradation of long-lived proteins, insoluble protein aggregates and invading microbes (18–21). We examined the co-localization of STING with the autophagy-related protein (Atg), ULK1 (a homologue of Atg1), Atg5, microtubule-associated protein 1 light chain (LC) 3 (a homologue of yeast Atg8), Atg9a, and Atg14L, since these are representative autophagy-related proteins in the four Atg complexes involved in the induction of autophagy (18–21). Among them, LC3 and Atg9a both show co-localization with STING after sensing dsDNA (Fig. 3*A* and *B* and Fig. S4 *A*–*C*). These results were unexpected, since the autophagy-related proteins tested here have been reported to localize at isolation membranes and autophagosomes (18–21). Surprisingly, subsequent characterization by electron microscopy revealed that the STING-positive puncta induced by dsDNA stimulation did not have morphological characteristics of autophagosomes, double-membrane-bound structures, but were unidentified membrane-bound compartments (Fig. 3*C* and Fig. S5). However, in unstimulated MEFs, STING-positive puncta were hardly observed and STING localized to the ER (Fig. 3*C* and Fig. S5). Atg7-mediated ubiquitin-like conjugation, an essential step for autophagosome formation, was not important for regulation of dsDNA-induced innate immune responses because cytokine production and translocation of STING normally occurred in Atg7-knockout MEFs following dsDNA stimulation (Fig. S6 *A* and *B*). IFN-β production was also normal in Atg16L1-knockout MEFs stimulated with dsDNA (Fig. S6*B*). These results clearly demonstrate that dsDNA stimulation drives the formation of STING-positive unique punctate structures and suggests that several autophagy-related proteins regulate dsDNA-induced innate immune responses independently of autophagy.

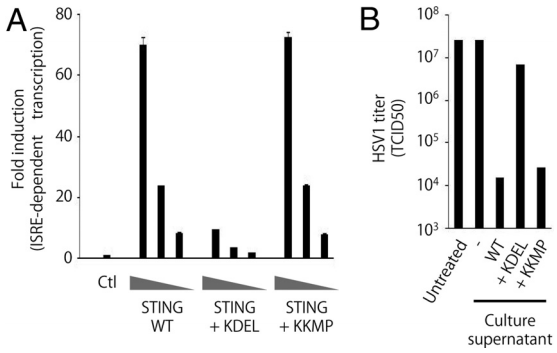

Fig. 2. The translocation of STING from ER facilitates to induce antiviral response. (*A*) Luciferase assay of lysates from 293 cells transfected with various amounts of the indicated STING expression vectors along with pISRE-Luc and pRL-TK. ISRE, IFN-stimulation responsive element. TK, thymidine kinase. Firefly luciferase activity was normalized to renilla luciferase activity to measure ISRE-dependent transcriptional activity. The results shown are means ± SD. (n = 3). (*B*) Anti-HSV1 activity in culture supernatants from 293 cells transfected with the indicated expression vectors for 24 h. HSV1 production [in 50% tissue culture infectious dose (TCID50)] was measured 24 h after infection of Vero cells either untreated or treated with the indicated culture supernatants.

Atg9a Is Required for Autophagy. Atg9a is the only multispanning membrane protein identified as an Atg protein in mammals (18–22). Although the precise molecular functions of the Atg9a protein are still unclear, Atg9a is proposed to mediate membrane transport to generate autophagosomes (18–22). It has been reported that Atg9a locates to the Golgi apparatus and to late endosomes and that Atg9a does not steadily reside at one site, but rather dynamically cycles between these organelles under starvation conditions (22). Since Atg9a co-localizes with STING after sensing dsDNA, we generated Atg9a mutant mice and examined the role of Atg9a in the regulation of dsDNA-induced innate immune responses as well as in autophagosome formation (Fig. S7 *A* and *B*). All Atg9a-knockout mice died within 1 day of delivery, indicating that Atg9a is essential for survival during neonatal starvation (Fig. S7*D*). This phenotype is similar to that

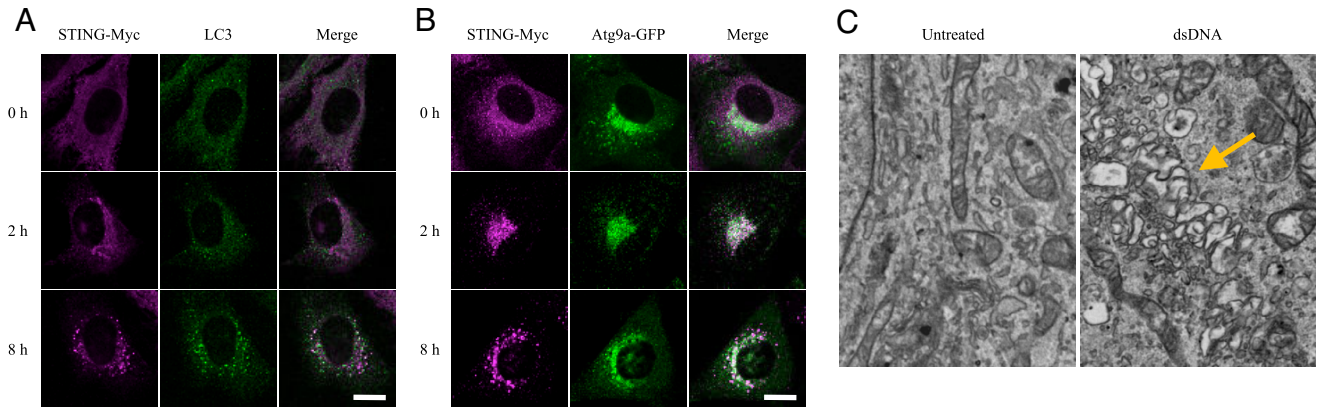

Fig. 3. STING colocalizes with Atg9a and assembles at unique membrane-bound compartments after dsDNA stimulation. (*A* and *B*) Wild-type MEFs stably expressing STING-Myc were transfected with poly (dA-dT) (1 μg/mL) for the indicated periods. The localization of STING and the indicated proteins was observed by confocal laser scanning microscopy. (Scale bars, 20 μm.) (*C*) Wild-type primary MEFs stably expressing STING-GFP were transfected with poly (dA-dT) for 8 h and then fixed. The cells were subjected to fluorescence-coupled electron microscopy. Yellow arrow indicates the STING -positive membrane-bound compartments.

observed in Atg5-, Atg7-, and Atg16L1-deficient mice (18–23). Although Atg9a is not necessary for Atg12 conjugation to Atg5, it is required for efficient LC3 conjugation to PE, an essential process for the formation of autophagosomes (Fig. S8*A*) (18–21). Consistently, formation of LC3 dots and autophagosomes was hardly observed in Atg9a-knockout MEFs under nutrient-starved conditions (Fig. S8 *B* and *D*). The loss of Atg9a results in a decrease in the bulk degradation of long-lived proteins and the massive accumulation of p62 (Fig. S8 *E* and *F*). Although Atg9a knockout MEFs express a deleted form of Atg9a mRNA lacking exon 6 to exon 11 (Fig. S7*C*), the expression of such a mutant mRNA seems not to affect the induction of autophagy in Atg9a-knockout MEFs because complementation of Atg9a-knockout MEFs with the Atg9a-GFP protein restores the ability to induce autophagy (Fig. S8*C*). These results indicate that Atg9a is an essential requirement for autophagy.

Atg9a Regulates dsDNA-Induced Innate Immune Response. We examined the role of Atg9a in regulating the localization of STING. While dsDNA-induced translocation of STING from the ER to the Golgi apparatus occurs normally in Atg9a-knockout MEFs, translocation of STING from the Golgi apparatus to the punctate structures, and the assembly of STING and TBK1 is greatly enhanced in Atg9a-knockout MEFs (Fig. 4). Consistently, dsDNA-induced phosphorylation of IRF3 is enhanced in Atg9a-knockout MEFs (Fig. 5*A*). Our data show that both the transcription of Ifn-β, Il-6, and Cxcl10, and the production of IFN-β are enhanced in Atg9a-knockout MEFs stimulated with dsDNA (Fig. 5 *B* and *C*). The enhanced production of IFN-β in Atg9a-knockout MEFs is normalized by retroviral transduction of Atg9a-GFP (Fig. S9). These results indicate that Atg9a limits dsDNA-induced innate immune responses by regulating the assembly of STING and TBK1.

Discussion

Increasing evidence has shown the critical role of autophagy-related proteins in the physiological and pathological conditions (18–21, 23–27). This study highlights a unique role for

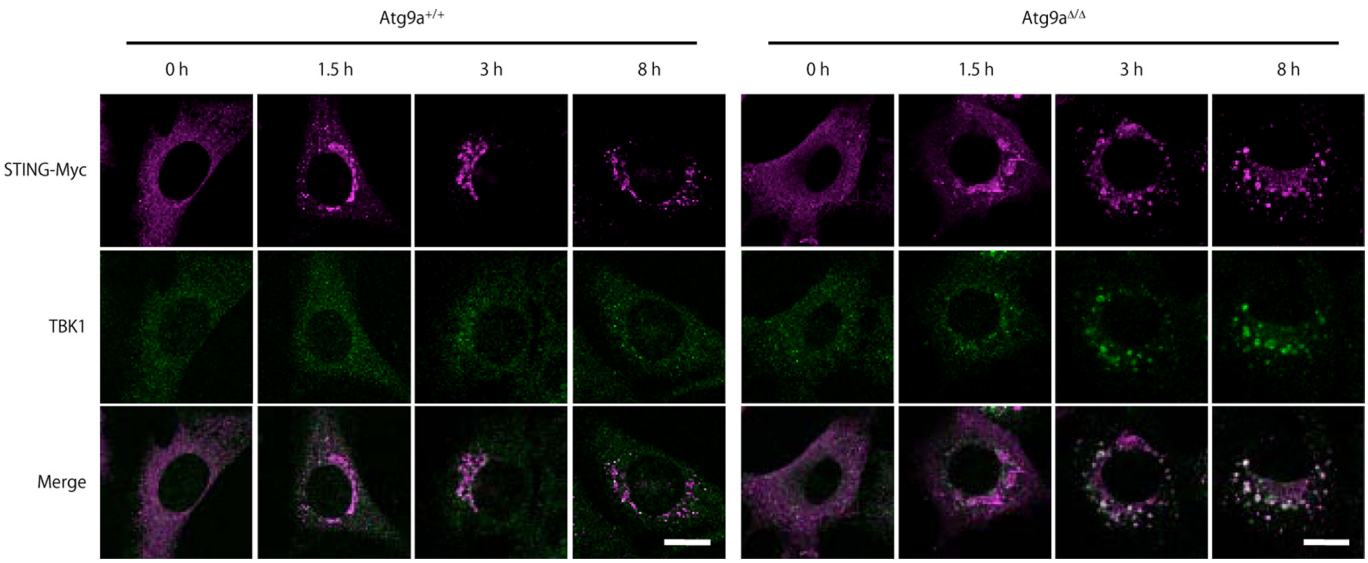

Fig. 4. Atg9a controls the assembly of STING and TBK1 after dsDNA stimulation. Atg9a$^{+/+}$ and Atg9a$^{\Delta/\Delta}$ primary MEFs stably expressing STING-Myc were transfected with poly (dA-dT) (1 μg/mL) for the indicated periods. The cells were fixed, immunostained with anti-Myc and anti-TBK1 antibodies and then observed by confocal laser scanning microscopy. (Scale bars, 20 μm.)

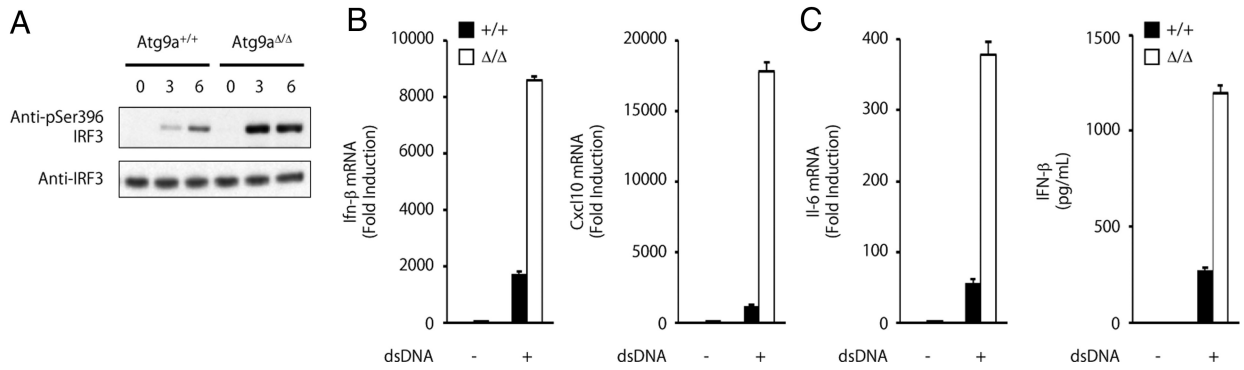

Fig. 5. Loss of Atg9a enhances dsDNA-induced innate immune response. (*A*) Immunoblots of lysates from Atg9a$^{+/+}$ and Atg9a$^{\Delta/\Delta}$ primary MEFs transfected with poly (dA-dT) for the indicated periods. The membranes were probed with the indicated antibodies. (*B*) Quantitative-RT-PCR of the indicated RNAs from Atg9a$^{+/+}$ and Atg9a$^{\Delta/\Delta}$ primary MEFs transfected with poly (dA-dT) for 8 h. The results shown are means ± SD. ($n = 3$). (*C*) Production of IFN-β by Atg9a$^{+/+}$ and Atg9a$^{\Delta/\Delta}$ primary MEFs transfected with poly (dA-dT) for 24 h. The results shown are means ± SD. ($n = 3$).

Atg9a in the regulation of the dsDNA-induced innate immune response. Although all autophagy-related proteins are necessary for the induction of autophagy, each autophagy-related protein acts as a distinct regulator of membrane traffic and is required for the differential steps of autophagosome formation (18–21). Therefore, it is possible that the distinct function of each autophagy-related protein contributes to certain types of cellular response in addition to autophagy. Indeed, the selective involvement of Atg9a in dsDNA-induced innate immune responses discloses that each autophagy-related protein does not always play the same role in immunity, but has distinct functions that regulate the immune system.

Recent studies have shown that the poly (dA-dT), B-form of dsDNA used in this study, induces RNA polymerase III-dependent innate immune responses both in human cells and in immortalized mouse cells (28, 29). However, it also has been reported that in primary mouse cells, B-form dsDNA induces innate immune responses independently of the RNA polymerase III-IFN-β promoter stimulator (IPS)-1 signaling axis (28–30). Enhanced B-form dsDNA-induced innate immune responses in Atg9a-knockout MEFs might be independent of the function of RNA polymerase III because we used primary MEFs in the experiments. We confirmed that the translocation of STING is induced by B-form dsDNA in both primary and immortalized mouse MEFs as well as in human cells (Figs. 1 and 4, and Fig. S3*C*). These results indicate that both the immortalization and species differences are unrelated to the translocation of STING driven by B-form dsDNA. Further studies are still needed to identify the dsDNA sensor responsible for the translocation of STING, and to understand the precise molecular mechanisms underlying dsDNA-induced signal transduction.

Materials and Methods

Reagents. Anti-phosphoSer396-IRF3 and anti-Myc antibodies were purchased from Cell Signaling Technology. Anti-IRF3 antibody was purchased from Santa Cruz Biotechnology. Recombinant mouse IFN-β and the ELISA kit for mouse IFN-β were purchased from PBL InterferonSource. ELISA kits for mouse CXCL10 and IL-6 were purchased from R&D Systems. Poly (dA-dT) was purchased from Sigma. Lipofectamine 2000 was purchased from Invitrogen.

Plasmids. pcDNA3.1 (+) was purchased from Invitrogen. pISRE-luc was purchased from Stratagene. pRL-TK was purchased from Promega. The expression constructs pMRX-ires-puro and pMRX-ires-bsr (kindly donated by Dr. S. Yamaoka) were derivatives of pMX (kindly donated by Dr. T. Kitamura), and have been described previously (31).

Complementary DNA encoding mouse Sting was inserted into pcDNA3, pMRX-ires-bsr and pMRX-GFP-ires-bsr, generating pcDNA3-Sting, pMRX-Sting-ires-bsr, and pMRX-Sting-GFP-ires-bsr, respectively. Complementary DNA encoding the transmembrane domain of Cyb5 was inserted into pMRX-GFP-MCS-ires-bsr, generating pMRX-GFP-ER-ires-bsr. Complementary DNA encoding the GFP and Atg9a were inserted into pMRX-ires-puro, generating pMRX-Atg9a-GFP-ires-puro.

Generation of Atg9a-Deficient Mice. The fragment of the Atg9a gene was isolated from genomic DNA extracted from wild-type ES cells by PCR. A targeting vector was constructed by replacing exons 6, 7, 8, 9, 10, and 11 with a neomycin-resistance gene cassette (neo), and a herpes simplex virus thymidine kinase driven by a PGK promoter was inserted into the genomic fragment to enable negative selection. After the targeting vector was transfected into ES cells, G418, and gancyclovir doubly resistant colonies were selected and screened by PCR and Southern blotting. Homologous recombinants were microinjected into C57BL/6 female mice, and heterozygous F1 progenies were intercrossed to obtain Atg9a-deficient mice. The Atg9a-deficient mice used were on a 129Sv × C57BL/6 background.

Mice were maintained in our animal facility and treated in accordance with the guidelines of Osaka University.

Mice, Cells, and Viruses. Mice deficient in Atg16L1 have been previously described[15]. Atg7-deficient mice were kindly donated by Drs. M. Komatsu and K. Tanaka. The Plat-E cells used for the generation of recombinant retrovirus were kindly donated by Dr. T. Kitamura (University of Tokyo, Tokyo, Japan). Retroviral infection was performed as previously described (31). Cells (293 and HeLa) were purchased from ATCC. Herpes simplex virus 1 was kindly donated by Dr. Kawaguchi (University of Tokyo, Tokyo, Japan).

Preparation of Mouse Embryonic Fibroblasts. Mouse embryonic fibroblasts were prepared as previously described (23).

RT-PCR. Total RNA was isolated using RNAeasy Mini kits (Qiagen) according to the manufacturer's instructions. Reverse transcription was performed using ReverTra Ace (TOYOBO) according to the manufacturer's instructions.

For quantitative PCR, cDNA fragments were amplified by RealTime PCR Master Mix (TOYOBO) according to the manufacturer's instructions. Fluorescence from the TaqMan probe for each cytokine was detected by a 7500 Real-Time PCR System (Applied Biosystems). To determine the relative induction of cytokine mRNA in response to dsDNA stimulation, the mRNA expression level of each gene was normalized to the expression level of 18S RNA. The experiments were repeated at least twice. The results were reproducible.

Immunoblotting. Immunoblotting were performed as previously described (23). The experiments were repeated at least three times. The results were reproducible.

ELISA. The level of cytokine production was measured by ELISA according to manufacturer's instructions. The experiments were repeated at least three times. The results were reproducible.

Fluorescence Microscopy. Immunocytochemistry analysis was performed as previously described (23, 32). Samples were examined under a fluorescence laser scanning confocal microscope, FV1000 (Olympus). The experiments were repeated at least twice. The results were reproducible.

Electron Microscopy Analysis. Electron microscopy analysis was performed as previously described (23). The experiments were repeated at least twice. The results were reproducible.

Materials and methods for SI figures are described in *SI Text*.

Note. While our manuscript was in submission, Ishikawa et al. (33) reported the translocation of STING from ER to EXOC2-positive compartments after dsDNA stimulation.

ACKNOWLEDGMENTS. We thank Drs. K. Tanaka, M. Komatsu, N. Mizushima, T. Kitamura, and Y. Kawaguchi for providing invaluable materials; the members of the Laboratory of Host Defense for discussion; M. Kumagai, N. Kitagaki, R. Abe, and Y. Fujiwara for technical assistance, and E. Kamada for secretarial assistance. This work was supported in part by grants from the Ministry of Education, Culture, Sports, Science, and Technology of Japan; the Ministry of Health, Labor, and Welfare of Japan; and the 21st Century Center of Excellence Program of Japan, and by National Institutes of Health Grant AI070167 (to S.A).

1. Palm NW, Medzhitov R (2009) Pattern recognition receptors and control of adaptive immunity. *Immunol Rev* 227:221–233.
2. Beutler B (2009) Microbe sensing, positive feedback loops, and the pathogenesis of inflammatory diseases. *Immunol Rev* 227:248–263.
3. Kawai T, Akira S (2009) The roles of TLRs, RLRs and NLRs in pathogen recognition. *Int Immunol* 21:317–337.
4. Ishii KJ, et al. (2006) A Toll-like receptor-independent antiviral response induced by double-stranded B-form DNA. *Nat Immunol* 7:40–48.
5. Stetson DB, Medzhitov R (2006) Recognition of cytosolic DNA activates an IRF3-dependent innate immune response. *Immunity* 24:93–103.
6. Ishii KJ, et al. (2008) TANK-binding kinase-1 delineates innate and adaptive immune responses to DNA vaccines. *Nature* 451:725–729.
7. Charrel-Dennis M, et al. (2008) TLR-independent type I interferon induction in response to an extracellular bacterial pathogen via intracellular recognition of its DNA. *Cell Host Microbe* 4:543–554.
8. Schroder K, Muruve DA, Tschopp J (2009) Innate immunity: Cytoplasmic DNA sensing by the AIM2 inflammasome. *Curr Biol* 19:R262–R265.
9. Hornung V, et al. (2009) AIM2 recognizes cytosolic dsDNA and forms a caspase-1-activating inflammasome with ASC. *Nature* 458:514–518.
10. Kawane K, et al. (2006) Chronic polyarthritis caused by mammalian DNA that escapes from degradation in macrophages. *Nature* 443:998–1002.
11. Stetson DB, Ko JS, Heidmann T, Medzhitov R (2008) Trex1 prevents cell-intrinsic initiation of autoimmunity. *Cell* 134:587–598.
12. Jin L, et al. (2008) MPYS, a novel membrane tetraspanner, is associated with major histocompatibility complex class II and mediates transduction of apoptotic signals. *Mol Cell Biol* 28:5014–5026.
13. Ishikawa H, Barber GN (2008) STING is an endoplasmic reticulum adaptor that facilitates innate immune signaling. *Nature* 455:674–678.
14. Zhong B, et al. (2008) The adaptor protein MITA links virus-sensing receptors to IRF3 transcription factor activation. *Immunity* 29:538–550.
15. Sun W, et al. (2009) ERIS, an endoplasmic reticulum IFN stimulator, activates innate immune signaling through dimerization. *Proc Natl Acad Sci USA* 106:8653–8658.
16. Komatsu M, et al. (2007) Homeostatic levels of p62 control cytoplasmic inclusion body formation in autophagy-deficient mice. *Cell* 131:1149–1163.
17. Stornaiuolo M, et al. (2003) KDEL and KKXX retrieval signals appended to the same reporter protein determine different trafficking between endoplasmic reticulum, intermediate compartment, and Golgi complex. *Mol Biol Cell* 14:889–902.
18. Xie Z, Klionsky DJ (2007) Autophagosome formation: Core machinery and adaptations. *Nat Cell Biol* 9:1102–1109.
19. Nakatogawa H, Suzuki K, Kamada Y, Ohsumi Y (2009) Dynamics and diversity in autophagy mechanisms: Lessons from yeast. *Nat Rev* Mol Cell Biol 10:458–467.
20. Mizushima N, Levine B, Cuervo AM, Klionsky DJ (2008) Autophagy fights disease through cellular self-digestion. *Nature* 451:1069–1075.
21. Deretic V, Levine B (2009) Autophagy, immunity, and microbial adaptations. *Cell Host Microbe* 5:527–549.
22. Webber JL, Young AR, Tooze SA (2007) Atg9 trafficking in mammalian cells. *Autophagy* 3:54–56.
23. Saitoh T, et al. (2008) Loss of the autophagy protein Atg16L1 enhances endotoxin-induced IL-1beta production. *Nature* 456:264–268.
24. Cadwell K, et al. (2008) A key role for autophagy and the autophagy gene Atg16l1 in mouse and human intestinal Paneth cells. *Nature* 456:259–263.
25. Lee HK, Lund JM, Ramanathan B, Mizushima N, Iwasaki A (2007) Autophagy-dependent viral recognition by plasmacytoid dendritic cells. *Science* 315:1398–1401.
26. Jounai N, et al. (2007) The Atg5 Atg12 conjugate associates with innate antiviral immune responses. *Proc Natl Acad Sci USA* 104:14050–14055.
27. Tal MC, et al. (2009) Absence of autophagy results in reactive oxygen species-dependent amplification of RLR signaling. *Proc Natl Acad Sci USA* 106:2770–2775.
28. Ablasser A, et al. (2009) RIG-I-dependent sensing of poly(dA:dT) through the induction of an RNA polymerase III-transcribed RNA intermediate. *Nat Immunol*.
29. Chiu YH, Macmillan JB, Chen ZJ (2009) RNA Polymerase III detects cytosolic DNA and induces Type I interferons through the RIG-I pathway. *Cell* 138:576–591.
30. Sun Q, et al. (2006) The specific and essential role of MAVS in antiviral innate immune responses. *Immunity* 24:633–642.
31. Saitoh T, et al. (2003) TWEAK induces NF-kappaB2 p100 processing and long lasting NF-kappaB activation. *J Biol Chem* 278:36005–36012.
32. Matsunaga K, et al. (2009) Two Beclin 1-binding proteins, Atg14L and Rubicon, reciprocally regulate autophagy at different stages. *Nat Cell Biol* 11:385–396.
33. Ishikawa H, Ma Z, Barber GN (2009) *Nature* 461:788–792.